FISEVIER

Contents lists available at ScienceDirect

Journal of Colloid and Interface Science

journal homepage: www.elsevier.com/locate/jcis



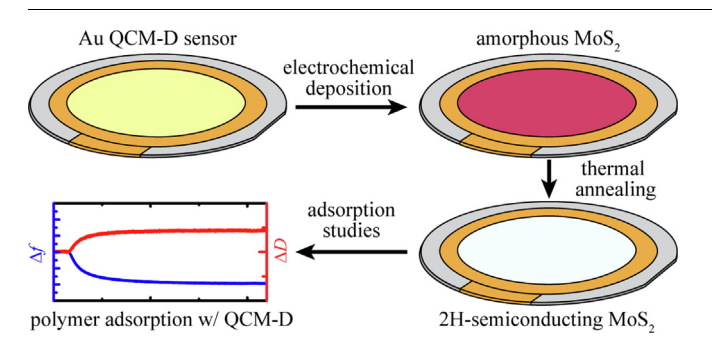
Electrochemically deposited molybdenum disulfide surfaces enable polymer adsorption studies using quartz crystal microbalance with dissipation monitoring (QCM-D)



Christopher S. O'Bryan ^{a,b,c}, Joseph Rosenfeld ^a, Aria Zhang ^b, Austin W. Keller ^b, Denis Bendejacq ^d, Cherie R. Kagan ^{b,e,f}, Christopher B. Murray ^{b,f}, Daeyeon Lee ^{a,*}, Russell J. Composto ^{b,c,*}

- ^a Department of Chemical and Biomolecular Engineering, University of Pennsylvania, Philadelphia, PA, United States
- ^b Department of Materials Science and Engineering, University of Pennsylvania, Philadelphia, PA, United States
- ^cLaboratory for Research on the Structure of Matter, University of Pennsylvania, Philadelphia, PA, United States
- d Complex Assemblies of Soft Matter Laboratory, IRL 3254, Solvay USA Inc., Bristol, PA, United States
- ^e Department of Electrical and Systems Engineering, University of Pennsylvania, Philadelphia, PA, United States
- ^f Department of Chemistry, University of Pennsylvania, Philadelphia, PA, United States

G R A P H I C A L A B S T R A C T



ARTICLE INFO

Article history:
Received 2 September 2021
Revised 21 December 2021
Accepted 16 January 2022
Available online 22 January 2022

Keywords:
Molybdenum disulfide
MoS2
Quartz Crystal Microbalance
QCM-D
Polymer adsorption
Dextran Adsorption
Electrochemical deposition
ECD
Froth Flotation
Mineral processing
Flotation Recovery

ABSTRACT

Polymer and small molecules are often used to modify the wettability of mineral surfaces which facilitates the separation of valuable minerals such as molybdenum disulfide (MoS₂) from gangue material through the process of froth flotation. By design, traditional methods used in the field for evaluating the separation efficacy of these additives fail to give proper access to adsorption kinetics and molecule conformation, crucial aspects of flotation where contact times may not allow for full thermodynamic equilibrium. Thus, there is a need for alternative methods for evaluating additives that accurately capture these features during the adsorption of additives at the solid/liquid interface. Here, we present a novel method for preparing MoS₂ films on quartz crystals used for Quartz Crystal Microbalance with Dissipation (QCM-D) measurements through an electrochemical deposition process. The resulting films exhibit well-controlled structure, composition, and thickness and therefore are ideal for quantifying polymer adsorption. After deposition, the sensors can be annealed without damaging the quartz crystal, resulting in a phase transition of the MoS₂ from the as-deposited, amorphous phase to the 2H semiconducting phase. Furthermore, we demonstrate the application of these sensors to study the interactions of additives at the solid/liquid interface by investigating the adsorption of a model polymer, dextran, onto both the amorphous and crystalline MoS2 surfaces. We find that the adsorption rate of dextran onto the amorphous surface is approximately twice as fast as the adsorption onto the annealed surface. These

^{*} Corresponding authors at: Department of Materials Science and Engineering, University of Pennsylvania, Philadelphia, PA, United States (R.J. Composto). E-mail addresses: daeyeon@seas.upenn.edu (D. Lee), composto@seas.upenn.edu (R.J. Composto).

studies demonstrate the ability to gain insight into the short-term kinetics of interaction between molecules and mineral surface, behavior that is key to designing additives with superior separation efficiency.

© 2022 Elsevier Inc. All rights reserved.

1. Introduction

Within the mineral industry, the separation of desired ore from gangue materials is commonly achieved through the process of froth flotation in which air bubbles released into a mineral slurry harvest the desired mineral by leveraging differences in surface wettability [1]. Hydrophobic particles attach to air bubbles moving through the slurry and are floated to the surface while hydrophilic particles settle to the bottom of the collection chamber. Often, polymers, small molecules, or nanoparticles may be added to selectively modify the surface wettability and promote flotation of a desired mineral by increasing hydrophobicity (collectors), or to suppress flotation by increasing hydrophilicity (suppressors) [2– 5]. For example, the separation of molybdenum disulfide (molybdenite; MoS₂), a naturally occurring hydrophobic mineral commonly mined with other copper sulfides, often requires a twostep flotation process in which a preliminary flotation is used to separate the molybdenite and copper sulfide minerals from the gangue minerals followed by a second flotation to separate the molybdenite from the other sulfide minerals [6-8]. Polymeric or small molecule additives may be added during the secondary flotation to selectively suppress the flotation of one of the sulfide containing minerals. The efficacy of these additives depends on the properties of the surface layer, rate of adsorption, and mineral selectivity [3,9,10]. However, explorations of these additives generally rely on small-batch flotation recovery measurements and ex situ imaging of the surface after adsorption to determine the rate of adsorption and surface coverage [9-13]. An in situ method for measuring the adsorption of polymers and small molecule additives onto the desired mineral surface would greatly enhance the ability to screen potential candidates for flotation suppressants and collectors.

Quartz Crystal Microbalance with Dissipation monitoring (QCM-D) is a surface sensitive method for measuring the adsorption of polymer and small molecule onto a desired surface in situ [14]. Recently, QCM-D measurements have been utilized to understand the adsorption rates and conformation of collector/suppressor polymer candidates [15-19]. These studies have generally relied on the modification of the quartz crystal surface to either directly match or mimic the desired mineral surface. For example, gold QCM-D sensors have been coated with an alkane-based selfassembled monolayer to study the hydrophobic interactions present in the adsorption of dextrin additives used in flotation studies [15]. Alternatively, more advanced deposition methods, including physical vapor deposition [17], electrospray deposition [20], atomic layer deposition [21], and electrochemical deposition [22], have been utilized to deposit sulfide mineral films onto OCM-D sensors. Although several of these deposition approaches have been used to deposit MoS₂ films, the application of these MoS₂ coated QCM-D sensors to perform systematic polymer adsorption studies has not been demonstrated. A method for preparing well-defined, uniform MoS2 films on QCM-D sensors and demonstrating their capacity to perform polymer adsorption studies would enable systematic explorations of new polymeric candidates to improve mineral separation and recovery during froth flotation.

Here, we present an electrodeposition method for preparing QCM-D sensors with robust MoS₂ films, which in turn enable polymer adsorption studies of importance for froth flotation

applications. Molybdenum disulfide films are prepared through an electrochemical deposition method onto Au QCM-D sensors with thicknesses ranging from \sim 50–500 nm and surface roughness below 4 nm. By developing a pulse deposition approach based on computational modeling of the solute concentration within the OCM-D flow cell, we achieve near uniform film deposition across the surface of the QCM-D sensor (14 mm diameter). In addition, we find this deposition process to be reversible, allowing individual QCM-D sensors to be reused to create fresh molybdenum disulfide films for polymer adsorption studies. Annealing of the sensors at 500 °C results in a phase transition from the as-deposited amorphous state to the semiconducting 2H phase. Furthermore, we demonstrate the application of these sensors to study polymeric adsorption by measuring the adsorption isotherms of dextran (40,000 g/mol) onto both the amorphous and semiconducting surfaces. Whereas the rate of adsorption on MoS2 increases with polymer concentration for both MoS₂ films, the adsorption rate of the dextran onto the amorphous surface is approximately twice as fast as adsorption onto the crystalline surface.

2. Methods and materials

2.1. Materials

Gold coated quartz QCM-D sensors were purchased from Nanoscience Instruments (Qsensors QSX301). 99.97% trace metal basis ammonium tetrathiomolybdate was purchased from Sigma Aldrich (323446). Dextran from *Leuconostoc mesenteroides* with an average molecular weight of 40,000 g/mol was purchased from Sigma-Aldrich (D1662). All materials were used as received unless otherwise noted.

2.2. Quartz crystal microbalance with dissipation monitoring

All quartz crystal microbalance with dissipation monitoring measurements are performed using a Q-sense Analyzer instrument. A quartz crystal decorated with two electrodes placed on either side is used as the resonating sensor with the desired material surface placed on top of one of the electrodes (Fig. 1a). By leveraging the inverse-piezoelectric effect, the quartz crystal is sheared when an oscillatory voltage is applied across the electrodes; when the frequency of the applied voltage matches the acoustic resonance frequency of the quartz crystal, the amplitude of the oscillation increases, resulting in an increase in the electrical current of the system [23,24]. The adsorption of polymers and small molecules onto the surface of the QCM-D sensor results in an increase in the thickness of the quartz crystal and thus a shift in the acoustic resonance frequency. When the adsorbed mass is small relative to the mass of the quartz crystal, evenly distributed across the surface, and rigidly bound, the frequency shift can be related to the area mass density of the adsorbed material through the Sauerbrey equation, $\Delta f=-rac{2f_0^2}{\sqrt{
ho_g c_q'}}rac{\Delta m}{A}$, where Δf is the shift in

the resonance frequency, f_0 is the resonance frequency of the fundamental mode, ρ_q is the density of the quartz crystal, G_q' is the elastic shear modulus of the quartz crystal, Δm is the change in the adsorbed mass, and A is active area of the piezoelectric sensor [23,24]. Furthermore, dissipation effects of the adsorbed material can be monitored by turning off the applied oscillation and

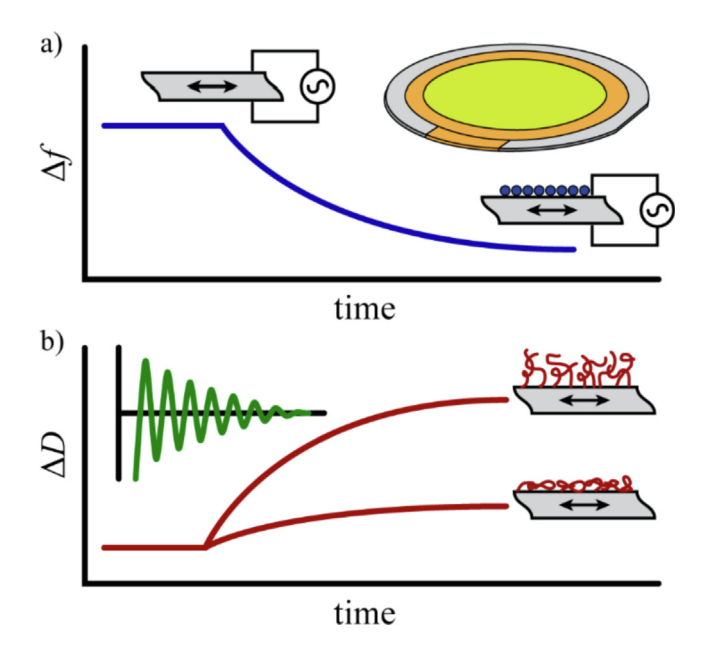


Fig. 1. Quartz Crystal Microbalance with Dissipation (QCM-D) is a highly surface sensitive method for measuring the adsorption of polymers and small molecules onto a surface. **a)** Adsorption of polymers and small molecules onto the surface of the QCM-D sensor increases the effective thickness of the quartz, resulting in a negative shift in the resonance frequency. This frequency shift can be related to the adsorbed mass density through the Sauerbrey equation. **b)** Insight into the polymer conformation on the surface is gathered from the shift in dissipation which is sensitive to the viscous component of the adsorbed layer; tightly bound polymer layers result in a smaller shift in dissipation as compared to a polymer in a 'floppier' conformation.

monitoring the energy loss of the system (Fig. 1b). This dissipation effect relates the ratio of energy loss per cycle to the total energy stored in the system, that is $D = E''/2\pi E'$ where E'' is the loss modulus and E' is the storage modulus [24]. Thus, the dissipation effects can be used to understand the conformation of the adsorbed surface. For example, a tightly bound polymer layer will result in less energy loss per cycle, and thus a smaller shift in the dissipation compared to a polymer layer that takes on a brush conformation with a higher loss modulus.

2.3. Electrochemical deposition of MoS₂ surfaces

Electrochemical depositions of molybdenum disulfide surfaces are performed using an electrochemical QCM-D flow cell (Qsense; QEM 401) and a Q-sense Analyzer instrument. Prior to deposition, the Au QCM-D sensor is cleaned using UV-Ozone for 30 min in a UV/Ozone ProCleaner Plus (Bioforce Nanosciences). The Au QCM-D sensor is then loaded into the electrochemical cell and equilibrated in deionized (DI) water until the drift in the measured frequency is < 1 Hz/hr. Next, a solution of ammonium tetrathiomolybdate is pumped into the electrochemical flow cell at the desired flow rate; fresh solutions of ammonium tetrathiomolybdate are prepared in DI water at the desired concentration and sonicated for 1 h before each deposition. Once the frequency shift of the Au QCM-D sensor has reached equilibrium, a -1V potential is applied across the surface to drive the deposition of the molybdenum disulfide using a National Instruments USB6009 bus-powered multifunctional data acquisition device (Fig. S1). After 20 min, the voltage is set to 0 V and the ammonium tetrathiomolybdate solution is replace with DI water.

The deposition of molybdenum disulfide using the pulse deposition approach is performed following a similar procedure using a VersaSTAT Series Potentiostat to apply the voltage potential. The potentiostat is programmed to follow a repeating square voltage

pattern in which a -1 V potential is applied for 5 s followed by 0 V for 45 s for 20 cycles. After the Au sensor has reached equilibrium in the ammonium tetrathiomolybdate solution (drift in the measured frequency of < 1 Hz/hr), the peristaltic pump is programmed to follow the desired pumping profile: 300 μ L/min for 30 s followed by a 20 s pause. After one pumping cycle, the potentiostat program is started and the molybdenum disulfide is deposited onto the Au OCM-D sensor.

2.4. Polymer adsorption measurements

All polymer adsorption measurements are performed using a Q-sense Analyzer QCM-D instrument. Prior to adsorption studies, the MoS $_2$ coated QCM-D sensors are loaded into the QCM-D flow cell and equilibrated in the appropriate buffer solution overnight until the drift in the measured frequency is < 1 Hz/hr. Once equilibrated, adsorption studies are performed by pumping the desired polymer solution into the flow cell for 30 min at a flow rate of 50 μ L/min and capturing the first 7 harmonics. After 30 min, the polymer solution is replaced by the buffer solution and the harmonics are monitored for an additional 15 min. All solutions are pumped into the QCM-D flow cell using a peristaltic pump. Adsorption studies are performed using dextran from *Leuconostoc mesenteroides* with an average molecular weight of 40,000 g/mol.

2.5. Sample characterization

Atomic Force Microscopy (AFM) imaging of the molybdenum disulfide surfaces is performed using a Bruker Icon AFM. AFM images are captured using the soft tapping mode. Raman spectroscopy characterization is performed using a Raman-NSOM confocal setup using a 532 nm excitation laser with a dwell time of 300 s.

X-ray diffraction (XRD) experiments are conducted using a Rigaku SmartLab X-ray diffractometer with a 3-kW sealed tube copper source operated at 40 kV and 44 mA using a parallel beam (PB) setup. For the incident optics, the parallel slit collimator (PSC) is set to 5.0°, the incident slit is set to 1.0 mm, and a length limiting incident slit of 10 mm is used. On the receiving optics side, the receiving slits RS1 and RS2 are both left open at 20.0 mm, and a 0.5-degree parallel slit analyzer (PSA) is used with the soller slit set to 5.0°. The attenuator is set to "auto" and the SC-70 detector (point counter) is used. For the grazing incidence (GI-XRD) experiments, omega is fixed and set to 0.5°, and the detector scan (20) is conducted in step mode from $10^{\circ}-60^{\circ}$ with a step size of 0.02° and a dwell time of 15.0 s.

Scanning Electron Microscopy (SEM) cross-sectional images of molybdenum disulfide films are captured using a TESCAN S8000X FIB/SEM. Images are captured using the ultra-high-resolution mode with a 5 kV, 100 pA electron beam.

2.6. Modeling solute concentration and deposition in QCM-D flow cell

Simulation of flow through the QCM-D cell is performed using the CFD module of COMSOL Multiphysics. The flow field is calculated using the laminar flow physics interface while neglecting gravity, and transport of the solute through the cell is calculated using the transport of diluted species physics interface. The geometry of the flow cell is modeled as a cylinder (radius = 5.625 mm; height = 0.4 mm) with the inlet and outlet of the cell positioned above and below the center of the cylindrical cell on the bottom surface (Fig. S2). Simulations are conducted at room temperature and the material properties of the fluid (density and viscosity) are taken to be that of water. For the flow field, the equations solved are the Navier-Stokes and continuity equations, given by:

$$\rho \frac{\partial \mathbf{u}}{\partial t} + \rho (\mathbf{u} \cdot \nabla) \mathbf{u} = \nabla \cdot [-P\mathbf{I} + \mu (\nabla \mathbf{u} + (\nabla \mathbf{u})^T]$$

$$\rho \nabla \cdot \boldsymbol{u} = 0$$

where ρ , \boldsymbol{u} , P, and μ are the density, velocity, pressure, and viscosity respectively of the fluid, t is time, and \boldsymbol{I} is the identity tensor. At the inlet of the cell, a mass flow rate condition that corresponds to either 50 or 150 μ L/min is used, and the pressure at the outlet is set to zero. Transport of the ammonium tetrathiomolybdate through the cell is modelled as a dilute species with a diffusion coefficient of 1×10^{-9} m²/s. Convective species transport is modelled using the equations:

$$\frac{\partial c}{\partial t} + \nabla \cdot \boldsymbol{J} + \boldsymbol{u} \cdot \nabla c = 0$$

$$I = -D\nabla c$$

where c is the concentration of the species, and D is its diffusion coefficient. The velocity field variable is taken from the solution to the Navier-Stokes and continuity equations. At all boundaries other than the inlet and outlet, the no-flux and no-slip conditions are enforced. The initial species concentration is taken to be zero throughout the volume of the cell, and the species concentration at the flow cell inlet is set to 5 mM. Species deposition to the cell surface is modelled using the surface reactions physics interface as a surface reaction between the deposition surface and the bulk solute with a rate law that is first order with respect to the bulk solute with a rate coefficient of 0.01 m/s (R = kc with units of mol/m²/s), and is modelled according to the equations:

$$\frac{\partial c_s}{\partial t} + \nabla_t \cdot (-D_i \nabla_t c_s) = R_s$$

$$\theta = \frac{\sigma c_{\rm s}}{\Gamma_{\rm s}}$$

Where the product surface concentration is given by c_s , its surface diffusivity is D_i , and the reaction rate law is R_s . The fractional surface coverage of the product is given by θ , the surface site occupancy number is σ , and the density of surface sites is Γ_s . ∇_t represents the surface or tangential gradient vector. The reaction product surface diffusivity is set to zero to model deposition. The surface is assumed to have a density of sites of $2 \times 10^{-5} \text{ mol/m}^2$ with a site occupancy number of unity. For computational simplicity, COMSOL's pre-setting of an extremely coarse mesh is applied. A time dependent study is conducted using the GMRES solver. Snapshots of the surface reaction product concentration on the deposition surface are taken after 20 min to match the experimental conditions.

2.7. Data analysis

All data analysis and fitting is performed using Origin Graphing Pro Software version 8.5.

3. Results and discussion

3.1. Surface deposition

To enable *in situ* adsorption studies of polymers and small molecules onto molybdenum disulfide surfaces, we prepare MoS_2 films onto commercially available Au QCM-D sensors. Previous studies have demonstrated the ability to form MoS_2 films through a variety of different electrochemical deposition reactions from a single source precursor [22,25,26]. Here, we deposit the MoS_2 through a $2e^-$ reduction reaction of ammonium tetrathiomolybdate from a single precursor as given by $MoS_2^{2-}(aq) + 2e^- + 2H_2O(l) \rightarrow MoS_2(s) + 2SH^-$

 $(\underline{aq}) + 2OH^{-}(aq)$. The deposition of the molybdenum disulfide films is performed using an electrochemical deposition QCM-D flow cell connected to a bus-powered multifunctional data acquisition device. The Au QCM-D sensor is equilibrated in a 5 mM solution of ammonium tetrathiomolybdate at a flow rate of 150 μL/min. Deposition of molybdenum disulfide is initiated by applying a -1 V potential across the ECD cell for 20 min and monitor by observing shifts in the resonating frequencies and dissipation terms (Fig. 2a, b). While applying the voltage potential, we observe a negative shift in the acoustic resonance frequencies of the Au OCM-D sensor across all harmonics with a relatively small spread resulting in the harmonics overlapping, confirming the deposition of the molybdenum disulfide onto the Au surface. In addition, we observe a large positive shift of the dissipation factors and a broad spread between the various dissipation harmonics (Fig. 2b). The penetration depth of a harmonic above the surface of the crystal depends on the frequency of the harmonic; namely, higher harmonics probe closer to the surface of the Au electrode whereas lower harmonics probe farther from the electrode surface [27]. Thus, the large shifts of the dissipation factor at lower harmonics and broad spread between the dissipation harmonics indicate that the dissipation effects are more significant further from the surface of the Au electrode, consistent with a nonuniform deposition of the MoS₂. Visual inspections of the QCM-D sensors after deposition confirm the non-uniform deposition of the MoS₂ onto the QCM-D sensors; thicker layers of molybdenum disulfide can be observed on the QCM-D sensor near the inlet of the electrochemical cell as compared to the outlet of the cell (Fig. 2c,d). We repeat these depositions across a range of ammonium tetrathiomolybdate concentrations and find the frequency shift scales linearly with solute concentration (Fig. 2e,f). However, for all solute concentrations, a non-uniform thickness of MoS₂ across the sensor surface is observed.

We hypothesize that the variations in the thickness across the surface of the QCM-D sensor are a result of a non-uniformity in ammonium tetrathiomolybdate concentration within the flow cell due to its consumption via MoS2 deposition on the surface which competes with its convection. To test this hypothesis, we perform simulations of the MoS₂ deposition as ammonium tetrathiomolybdate is pumped into the ECD flow cell (Fig. 3a,b). Here, we model the flow cell as a cylinder containing a flow inlet and outlet along one of the cylindrical surfaces (Fig. S2). The deposition of the MoS₂ onto the crystal surface is modelled as a first order surface reaction between the crystal surface and the bulk solute with a surface diffusivity of 0. We find the highest surface concentration is observed near the inlet of the ECD flow chamber and decreases radially toward the outlet, resulting in a teardrop shape (Fig. 3a). Increasing the flow rate results in a more uniform surface coverage throughout the flow cell; however, gradients in the concentration are still observed near the edges of the flow cell on the outlet side (Fig. 3b). These predicted concentration gradients visually match the deposition patterns found on QCM-D sensors when depositing MoS₂ films under similar flow conditions (Fig. 3c,d). At low flow rates, we find the deposition localized under the inlet of the flow chamber and along the flow direction toward the outlet with minimal deposition occurring at the edge of the sensor (Fig. 3c). Similarly, at higher flow rates the film exhibits non-uniformity with the largest deposition and thickest film located under the inlet although the deposition extends to the outer edge of the QCM-D sensor (Fig. 3d). These results indicate that the time scale for the convective supply of the reagent is longer than that for the reaction, resulting in the transient non-uniform reagent concentration profile in the chamber and hence non-uniform deposition of MoS₂ that persists with time. Interestingly, we find that there is not a significant change in the measured frequency shift, that is the mass area density, with increasing flow rates (Fig. 3e).

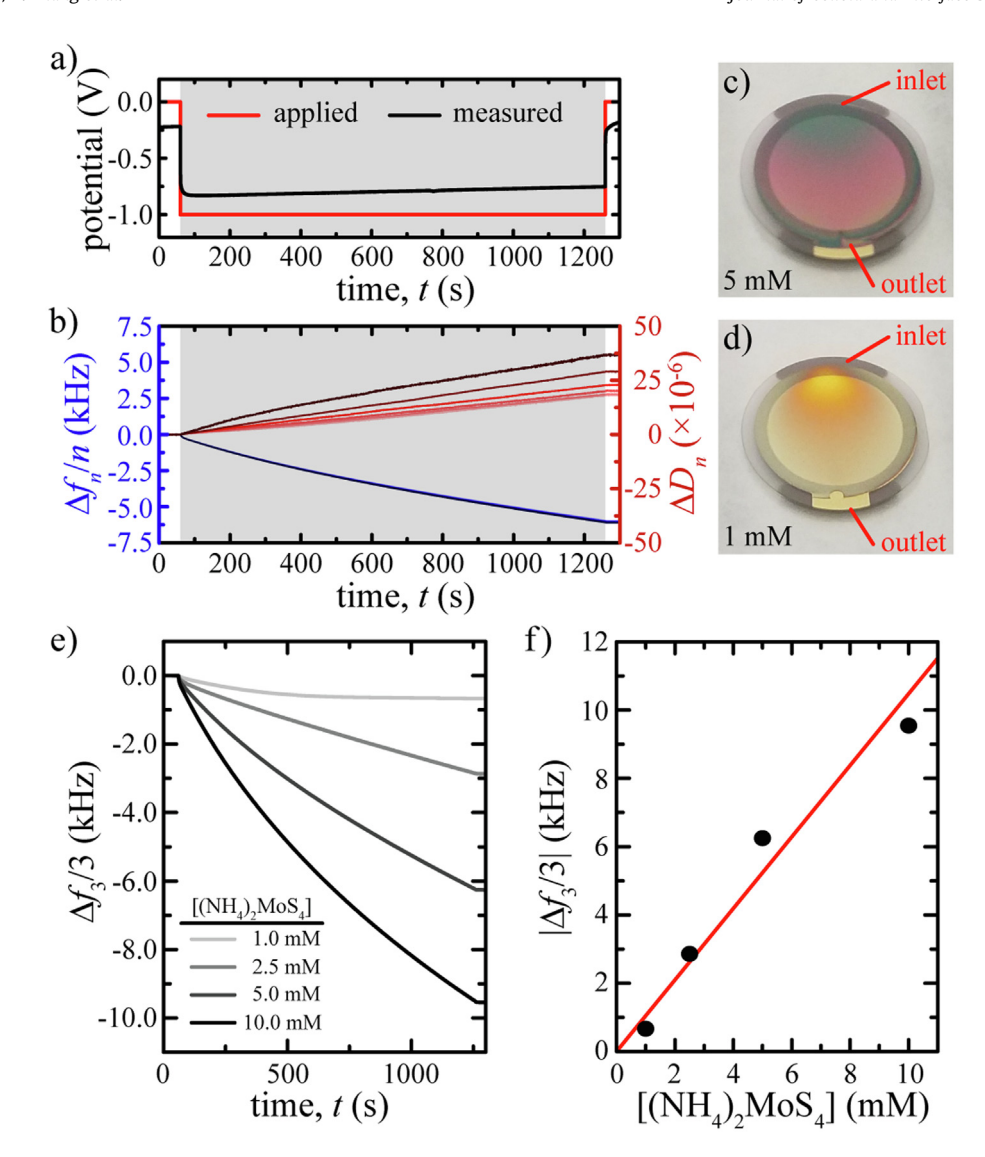


Fig. 2. Constant voltage deposition of MoS₂. a) Voltage profile for deposition MoS₂ onto Au QCM-D sensors. A constant -1 V potential is applied for 20 min. b) QCM-D measurements during the deposition of the MoS₂ from a 5 mM ammonium tetrathiomolybdate solution show a negative frequency shift (blue lines) corresponding to the added mass to the QCM-D sensor. The large shift in the dissipation terms (red lines) and the broad spread between the various harmonics indicate a non-uniform surface is deposited across the surface. Here we show the 3rd, 5th, 7th, 9th, 11th, and 13th harmonics arranged from darkest color to lightest color; solution concentration: 5 mM. c,d) Visual inspection of the QCM-D sensors after deposition confirms the non-uniform surface coverage of the MoS₂ with the most deposition occurring near the inlet of the flow chamber. These films are deposited from (c) 5 mM and (d) 1 mM ammonium tetrathiomolybdate solutions. QCM-D sensor diameter: 14 mm e) Depositions are repeated across a variety of ammonium tetrathiomolybdate concentrations. f) The total mass of MoS₂ deposited, indicated here by the magnitude of the shift in resonating frequency scales linearly with ammonium tetrathiomolybdate solution (line drawn to guide the eye).

Based on the observations from our simulations, we develop an alternative deposition approach in which we alternate between applying a voltage to drive the deposition and pumping in fresh ammonium tetrathiomolybdate solution into the flow chamber to achieve a uniform concentration. Simulations of solvent flowing into the flow cell without deposition occurring show that it takes ~ 90 s at a flow rate of 150 $\mu L/min$, or the equivalent fluid exchange of approximately four times the flow cell volume, to achieve a near-uniform solution concentration within the ECD flow cell (Fig. S3). Thus, we develop a pulse deposition approach in which the voltage is applied for 5 s followed by a 45 s pause during which fresh ammonium tetrathiomolybdate solution is pumped into the ECD flow chamber at 300 μ L/s for 30 s (\sim 4 \times the volume of the ECD flow cell) followed by a 20 s pause (Fig. 4a). This cycle is repeated 20 times to deposit molybdenum disulfide onto the surface of the Au QCM-D sensor. We find the change in frequencies measured during the pulse deposition approach to be similar to the continuous voltage deposition approach in Fig. 2f for similar deposition times. However, in contrast to the continuous voltage deposition, the resulting molybdenum disulfide surfaces from the pulse deposition have a uniform deposition pattern as indicated by the relatively small change in the dissipation factor and tight grouping between the dissipation harmonics (Fig. 4b). Most importantly, the film reflects a uniform color across the surface (Fig. 4c), consistent with a uniform thickness of molybdenum disulfide across the surface of the Au QCM-D sensor. The uniform thickness of the deposited layer lends itself to estimating the film thickness using the Sauerbrey model; we estimate the mass of the molybdenum disulfide layer deposited at a concentration of 5 mM to be $\sim 75~\mu g$. Fig. 4d shows that the estimated mass of the molybdenum disulfide increases linearly from $\sim 15~\text{to} \sim 160~\mu g$ as the concentration of solution increases from 1 to 10 mM, respectively.

A particularly unique aspect of this electrochemical approach is that the molybdenum disulfide deposition onto the quartz surface

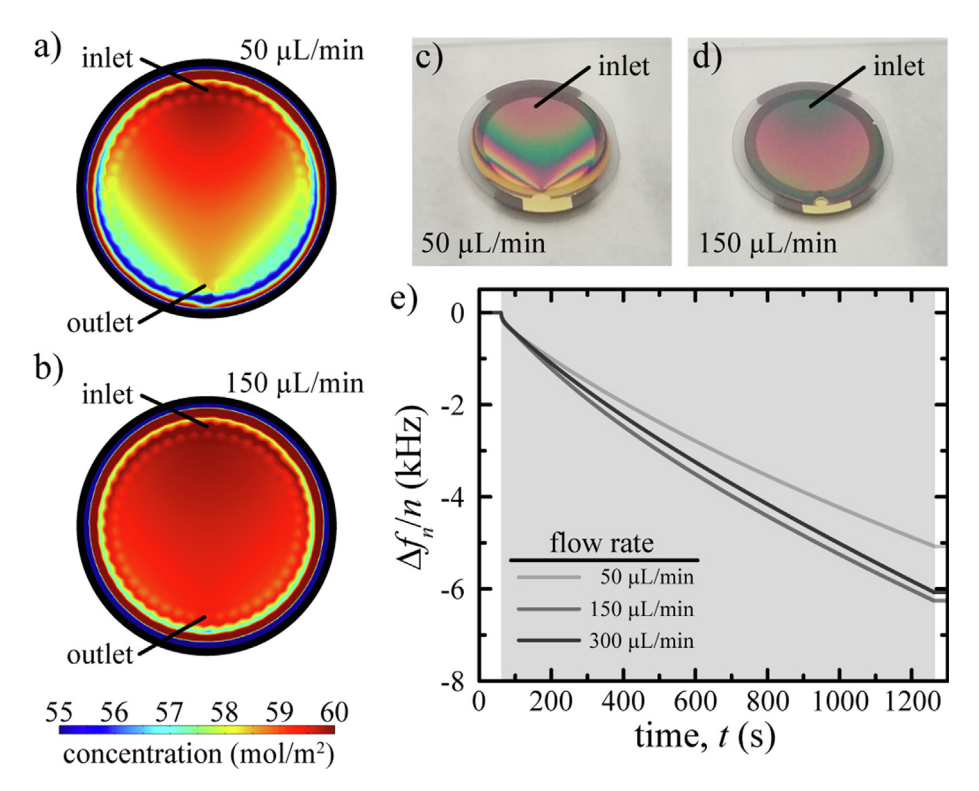


Fig. 3. MoS_2 deposition with varying flow rates. (a,b) Simulations of MoS_2 deposition onto the surface of the QCM-sensor show the emergence of concentration gradients resulting from the simultaneous deposition of MoS_2 onto the surface and the continuous flow of fresh ammonium tetrathiomolybdate solution into the flow chamber. Simulations were performed at flow rates of (a) 50 μ L/min and (b) 150 μ L/min. c,d) Similar deposition patterns are observed on QMC-D sensors with MoS2 films deposited under similar flow conditions suggesting that the non-uniform deposition patterns result from the concentration gradients of the ammonium tetrathiomolybdate inside the ECD flow cell. e) QCM-D results show that the decrease in resonating frequency representing the deposited mass does not strongly depend on the flow rate through the ECD flow cell.

is a reversible process. Recall that the deposition process shown in Fig. 4a was driven by applying a negative potential of -1V. Upon applying a positive voltage to the QCM-D sensor, a positive shift in the resonance frequency and a negative shift in the dissipation factors are observed, indicating the removal of mass (Fig. S4a). Here, we use a $1 \times PBS$ solution as the buffer solution during the dissolution process to provide free ions between the molybdenum disulfide film and the counter electrode and apply a continuous + 2 V potential for 7 min. We find that the positive shift in the resonating frequencies and negative shift in the dissipation factors measured during the dissolution of the MoS2 films are approximately equal in magnitude to the shifts measured during the initial film deposition (Fig. S4b). Visual inspection of the Au QCM-D sensors after removal shows no signs of residual molybdenum disulfide on the surface. After removing the molybdenum disulfide film, the QCM-D sensor can be reused and a new layer of MoS₂ can be deposited onto the QCM-D sensor (Fig. S4c). This process enables us to recycle previously used QCM-D sensors and to prepare fresh molybdenum disulfide films for polymer adsorption studies without the need to purchase new Au QCM-D sensors.

3.2. MoS₂ film characterization

To confirm that the deposited material is molybdenum disulfide, we perform Raman spectroscopy on the electro-deposited films (thickness ≈ 250 nm) using a 532 nm excitation laser and compare our results to the Raman spectrum of freshly exfoliated bulk crystalline MoS2. The bulk MoS2 (black) has two distinct peaks in the Raman spectrum at wavenumbers 383 cm $^{-1}$ and 407 cm $^{-1}$, corresponding with the in-plane E2g and out-of-plane A1g vibrational modes, respectively (Fig. 5a) [28]. Similar peak locations, however, are not observed for the as-deposited MoS2 films (blue)

(Fig. 5a). This observation suggests that the deposited film on the surface of the QCM-D sensor is an amorphous phase of molybdenum disulfide. To induce crystallization of the deposited material, we anneal the sensors at 500 °C for 1 h under argon gas in a 1-inch tube furnace. This annealing temperature is less than the quartz α - β phase transition temperature of 573 °C and frequency sweeps of the sensors after annealing show no indications of deterioration in the quality of the harmonic oscillators (Fig. S5) [23,29]. After annealing, the surface of the QCM-D sensor has a metallic appearance as seen in Fig. 5b. Furthermore, the Raman spectrum of the annealed film (red) has peak locations at 383 cm⁻¹ and 407 cm⁻¹, consistent with the bulk crystalline MoS₂ (black) (Fig. 5a).

To confirm that annealing converts MoS₂ from the amorphous to crystalline phase, we perform Grazing Incidence X-ray Diffraction (GI-XRD) on both the as-deposited (thickness ≈ 250 nm) and annealed (thickness ≈ 150 nm) films with a grazing incidence angle of 0.5° (Fig. 5c). For the as-deposited films (blue), we observe two peaks in the scattering intensity located at $2\theta = 38.3^{\circ}$ and 44.4°. However, similar peak locations are observed when performing GI-XRD on control samples of Au QCM sensors (green). These peak locations correspond with the (111) and (200) Bragg reflections of the gold surface suggesting the X-rays are penetrating through the as-deposited layer and scattering from the underlying substrate. The lack of additional peaks in the GI-XRD pattern of the as-deposited sample relative to the control sample indicate that the as-deposited film has an amorphous structure, in agreement with Raman spectroscopy results in Fig. 5a. After annealing (red), we observe the emergence of a diffraction peak at $2\theta = 14$. 4° consistent with the primary peak location observed in the control sample of a freshly exfoliated bulk MoS2 mineral (black) and corresponds to the (002) Bragg reflection of MoS₂. In addition,

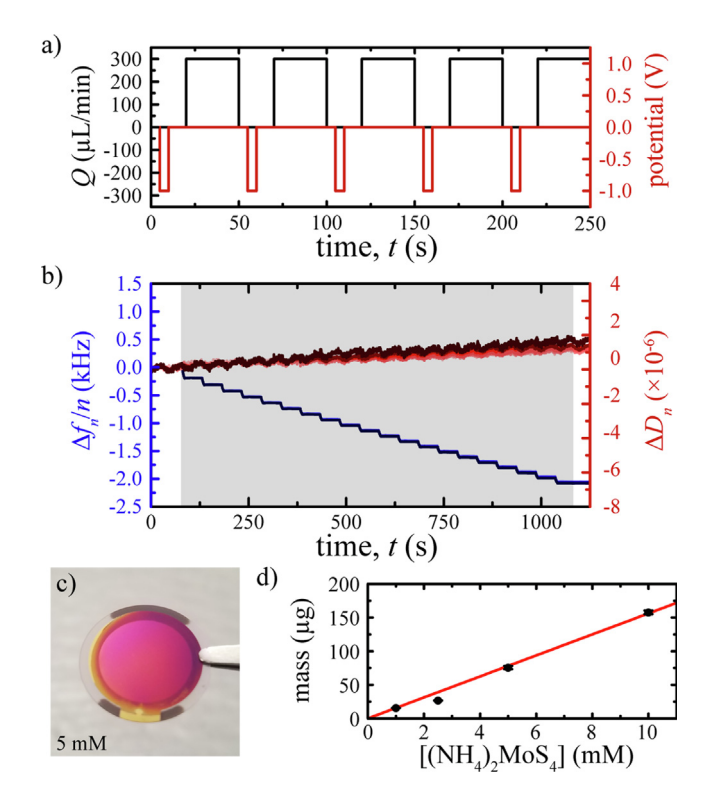


Fig. 4. Uniform MoS₂ films are deposited using a pulse deposition approach. **a)** The peristaltic pump is run for 30 s at 300 μL/min to replenish the ammonium tetrathiomolybdate solution in the ECD chamber followed by a 20 s pause. During this pause, a -1 V potential is applied across the surface for 5 s to deposit a layer of MoS₂ onto the gold surface. **b)** QCM-D plots of the frequency and dissipation shifts capture the deposition of the MoS₂ with each cycle. The relatively small change in dissipation and tight grouping of the harmonics indicate a tightly bound, uniform layer across the surface. The 3rd, 5th, 7th, 9th, 11th, and 13th harmonics are shown in order from the darkest color to lightest color; solution concentration: 5 mM. **c)** The pulse deposition approach results in a uniform deposition of the molybdenum disulfide across the surface of the QCM-D sensor. **d)** The estimated mass of the MoS₂ films calculated from the Sauerbrey equation after 20 deposition cycles as a function of ammonium tetrathiomolybdate concentration.

we observe a weaker peak locations near $2\theta = 33^{\circ}$ that we attributed to either the (100) $(2\theta = 32.7^{\circ})$ or the (101) $(2\theta = 33.5^{\circ})$ Bragg reflections. These results, in concert with Raman spectroscopy results suggest that the annealed sample is the 2H semiconducting phase of molybdenum disulfide [30].

To examine the surface morphology of the deposited molybdenum disulfide films, we perform tapping mode Atomic Force Microscopy (AFM) measurements on both as-deposited and annealed films (Fig. 5d,e). For the as-deposited film, height maps of the surface display small grains with diameters on the order of ~ 25 nm. The average RMS surface roughness (R_a) of the asdeposited surfaces is $R_q = 2.6$ nm. After annealing, we observe the formation of facets on the surface with feature sizes on the order of 100 nm. We attribute these facets to the crystallization and growth of the molybdenum disulfide grains as the Mo and S atoms order into basal planes. This formation of MoS2 crystals results in an increase in the surface roughness to R_q = 4.6 nm. Cross-sectional SEM images of molybdenum disulfide films deposited from a 5 mM solution of tetrathiomolybdate show a decrease in the thickness from 288.8 \pm 1.5 nm as-deposited to 177.4 \pm 2.1 nm after annealing (Fig. S6). Using our measurements of the deposited mass from the Sauerbrey equation (Fig. 4d), we calculate the density of the as-deposited and annealed films to increase from 2.32 g/cm³ to 4.1 g/cm³ We note that this calculated density is less than the density of MoS₂ mineral, ρ = 5.06 g/cm³, suggesting that the annealed samples are either not fully crystallized or not fully adopting a layered basal plane structure. We note that the total thickness of the MoS₂ layer can be tuned by the concentration of the ammonium tetrathiomolybdate during deposition or the total number of deposition cycles (Fig. 4b,d). For example, using the density values we determine here, we would predict the thickness of the MoS₂ layer deposited from a 2.5 mM solution of ammonium tetrathiomolybdate to be \sim 74.5 nm.

To examine the surface wettability, we perform advancing contact angle measurements of water droplets on the as-deposited and annealed films (Fig. S7). Naturally forming molybdenum disulfide minerals consists of inert basal planes held together through Van der Waals interactions resulting in a largely hydrophobic surface with active, hydrophilic edge sites [31]. We measure the advancing water contact angle of freshly exfoliated bulk molybde-

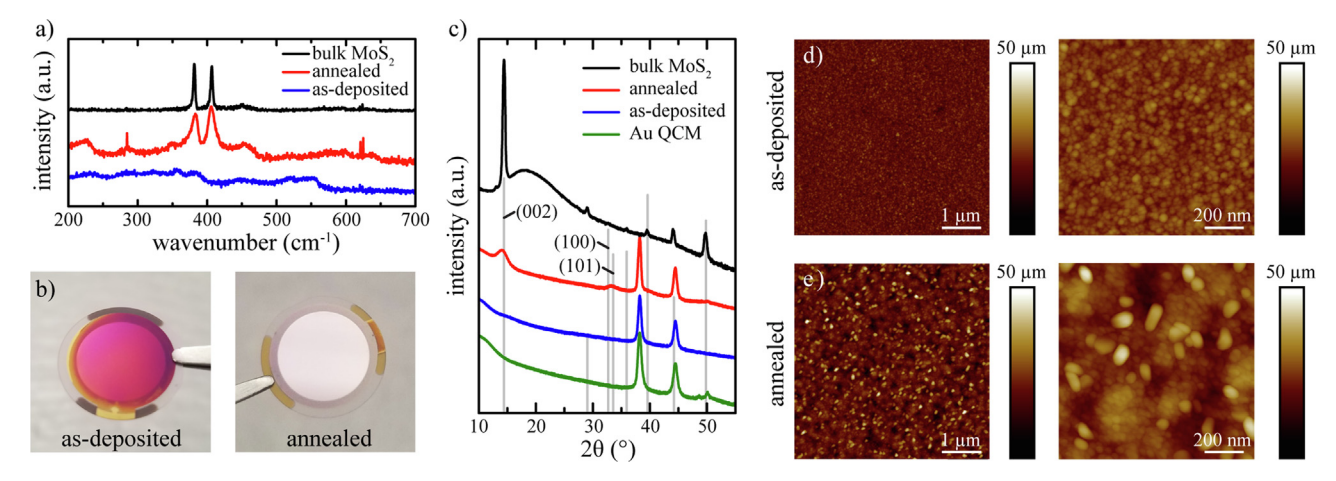


Fig. 5. Characterization of molybdenum disulfide bulk and film samples **a)** Raman spectroscopy measurements of the as-deposited MoS₂ surfaces do not contain the characteristic peaks of bulk MoS₂ mineral at wavenumbers 383 cm⁻¹ and 407 cm⁻¹, suggesting the formation of an amorphous phase. After annealing the MoS₂ film, peaks are observed in the Raman spectrum, suggesting a transition to the 2H semiconducting phase. **b)** Annealing of the MoS₂ QCM-D sensors results in a visual change in the surface to a metallic appearance. **c)** Grazing incidence X-ray diffraction confirms the transition from the amorphous to the 2H-semiconducting phase after annealing as indicated by the emergence of Bragg peaks at $2\theta = 14.4^{\circ}$ and near $2\theta = 32.7^{\circ}$ and 33.5° . **d)** AFM topography images of the as-deposited film show relatively smooth surfaces with surface roughness of $R_q = 2.6$ nm. **e)** After annealing, small facets form on the surface with lengths on the order of 100 nm resulting in an increase in surface roughness to $R_q = 4.6$ nm.

num disulfide surfaces to be $85.1^{\circ} \pm 3.8^{\circ}$. However, we find the advancing contact angle of as-deposited and annealed films to be lower than the bulk value, namely $67.5^{\circ} \pm 3.5^{\circ}$ and $69.4^{\circ} \pm 2.0^{\circ}$, respectively. We attribute this increase in surface wettability of the as-deposited films to the lack of formation of hydrophobic basal planes and the granular nature of the surface. Likewise, the granular nature of the annealed films presents an increased surface area for the hydrophilic edge sites as compared to the 2D bulk mineral structure, likely increasing the surface wettability.

3.3. Dextran adsorption studies

To demonstrate how these model molybdenum disulfide films can be used to study polymer adsorption, we investigate the adsorption dynamics of dextran (40 kDa), a highly branched polysaccharide, onto the as-deposited and annealed molybdenum disulfide surfaces. Previous investigations of similar polysaccharides adsorption onto hydrophobic mineral phases, including molybdenum disulfide, have proposed hydrophobic interactions as the main binding mechanism [10,32]. Here, each polymer adsorption measurement is performed on a freshly deposited, or annealed, molybdenum disulfide film. The sensor is equilibrated in DI water overnight to reach a baseline resonance frequency and a change in frequency of < 1 Hz/h. Polymer solution at a concentration of 50 µM is pumped through the QCM-D flow cell at a flow rate of 50 µL/min and the resulting shifts in frequency and dissipation are recorded. For the as-deposited films, we observe both a negative shift in the resonating frequency and a positive shift in the dissipation indicating that the dextran is adsorbing onto the surface (Fig. 6a). Furthermore, the overlap of the various harmonics indicates a nearly uniform adsorption of the polymer across the amorphous MoS₂ surface. After 2000 s, the polymer solution flowing through the chamber is replaced with DI water. During rinsing, we observe minimal changes in the frequency and dissipation shifts, indicating that the dextran remains adsorbed onto the molybdenum disulfide surface. Dextran adsorption is also measured on annealed MoS₂ films (Fig. 6b). A comparison of Fig. 6a and b shows that the dissipation changes are similar for the amorphous and crystalline MoS₂ cases; however, the larger change in frequency for adsorption on amorphous MoS₂ suggests greater dextran adsorption. Furthermore, these adsorption measurements confirm that the quartz sensors remain undamaged by the annealing process.

We repeat these polymer adsorption measurements across a range of dextran concentrations. We find that the rate at which the polymer adsorbs onto the molybdenum disulfide surface increases with increasing polymer concentration for both the asdeposited (Fig. 6c) and annealed (not shown) films. To quantify the rate at which the dextran adsorbs onto the molybdenum disulfide surfaces, the change in frequency is fit to a first-order Lang-

muir adsorption model. The change in the surface coverage, $\theta(t)$, is dependent on the adsorption rate of the polymer onto the surface (k_a) , the concentration of the polymer in solution (c), the current surface coverage of the polymer $(\theta(t))$, and the rate at which the polymer desorbs from the surface (k_d) , such that $\dot{\theta}(t) = k_a(1 - \theta(t))c - k_d(\theta(t))$. We assume that the surface coverage of the polymer is proportional to the shift in the frequency determined by the QCM-D measurements, that is $\Delta f(t) \approx \theta(t)$. Solving the differential equation for the frequency shift over time, we find that $\Delta f(t) = \Delta f_{ea} + Be^{-kt}$, where the decay constant $k = k_a c + k_d$. Thus, the adsorption and desorption rates of the dextran polymer onto the molybdenum disulfide surface can be determined by fitting an exponential decay to the OCM-D plots and fitting a line to the resulting decay constants k as a function of the polymer concentration. The equilibrium constant is then taken as the ratio of the rate of adsorption to the rate of desorption, that is $K_{eq} = k_a/k_d$

For each QCM-D plot, we fit an exponential function to the frequency shift profile over the first ~ 5 min to determine the decay

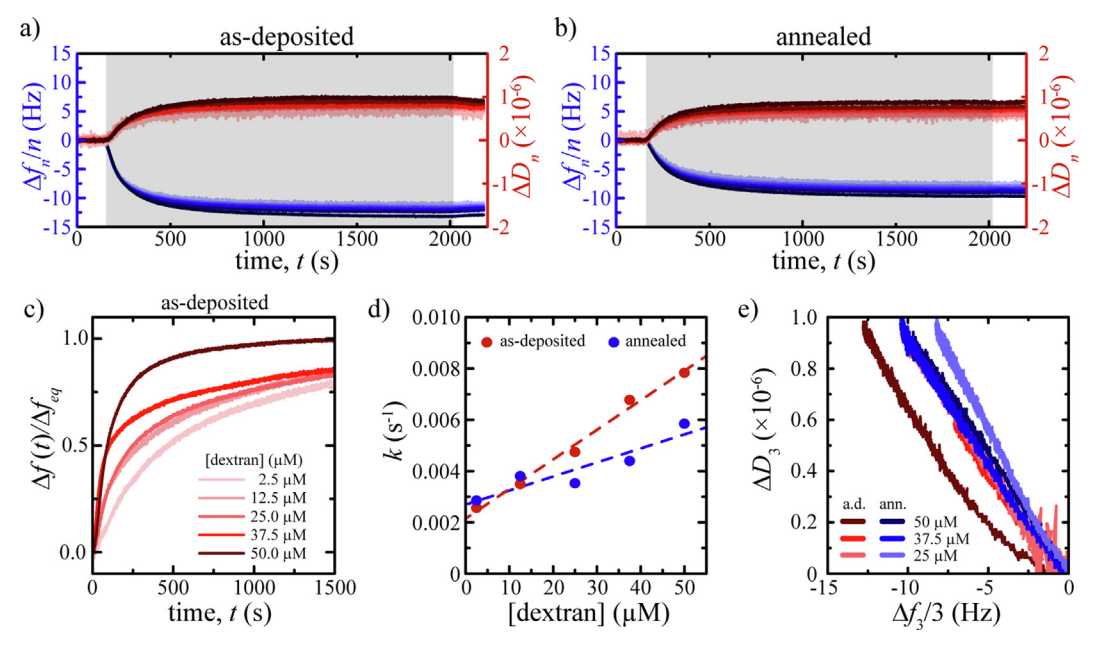


Fig. 6. QCM-D measurements of dextran adsorption onto MoS₂ surfaces. **a)** QCM-D adsorption measurements of 50 μM solutions of 40 k MW dextran onto as-deposited, amorphous molybdenum disulfide films. **b)** QCM-D adsorption measurements of 50 μM solutions of 40 k MW dextran onto annealed, 2H semiconducting phase molybdenum disulfide films. The 3rd, 5th, 7th, 9th, 11th, and 13th harmonics are shown in order from the darkest color to lightest color. **c)** Change in frequency versus time as dextran concentration increases from 2.5 μM to 50 μM. The rate of adsorption increases as dextran concentration increases. **d)** The rate of dextran adsorption is measured by fitting a first-order Langmuir model, $\Delta f(t) = \Delta f_{eq} + Be^{-kt}$, to the change in frequency over time. Here we plot the decay constant (k) vs the dextran concentration. The adsorption and desorption rates of dextran are determined using $k = k_a c + k_d$. **e)** Dissipation vs frequency shift plots indicate similar polymer conformation of the adsorbed dextran on both the as-deposited and annealed molybdenum disulfide surfaces. (Shown here are the 3rd harmonic).

constant, k (Fig. 6d). We measure the adsorption rate of dextran on the amorphous surface as $k_a = 1.15 \times 10^{-4} \, \mathrm{s}^{-1} \, \mu \mathrm{M}^{-1}$ and a desorption rate $k_d = 0.0022 \, \mathrm{s}^{-1}$, resulting in an equilibrium constant $K_{eq} = 52.3 \, \mathrm{mM}^{-1}$. We follow similar data analysis steps to measure the adsorption and desorption rates of dextran onto the annealed molybdenum disulfide surface and find $k_a = 0.55 \times 10^{-4} \, \mathrm{s}^{-1} \, \mu \mathrm{M}^{-1}$ and $k_d = 0.0027 \, \mathrm{s}^{-1}$, resulting in an equilibrium constant $K_{eq} = 20.4 \, \mathrm{mM}^{-1}$. Interestingly, while the adsorption rate of the dextran onto the amorphous surface is approximately twice as fast as the dextran adsorption onto the annealed surface, the desorption rate of the dextran is approximately equal for both surfaces.

In addition to the rate of the polymer adsorption, the changes in the conformation of the adsorbed polymer can be explored through the relationship between the dissipation shift and frequency shift. A linear relationship between the dissipation and frequency shifts indicates chain conformation remains the same as coverage increases (i.e., higher dextran concentration), while a discontinuity or change in slope indicates that the polymer chains rearrange their conformation. For example, if chains became more tightly bound as polymer adsorption increases, a shift to a smaller slope in dissipation at higher frequency shifts would occur. In this study, we observe a nearly linear relationship in the dissipation shift with increasing adsorbed mass for both the as-deposited and annealed surfaces, indicating that the dextran does not undergo a significant change in conformation with increased polymer adsorption (Fig. 6e, S8). Furthermore, we find the slope of the dissipation versus frequency to be similar for both surfaces, suggesting that the polymer adopts a similar conformation on both the as-deposited and annealed surfaces. In fact, we find that the adsorbed dextran results in similar changes in the contact angle of water droplets from $67.5^{\circ} \pm 3.5^{\circ}$ and $69.4^{\circ} \pm 2.0^{\circ}$ to $47.9^{\circ} \pm 0.7^{\circ}$ and $44.4^{\circ} \pm 3.8^{\circ}$ for the as-deposited and annealed surfaces, respectively (Fig. S7). Collectively, we interpret these results to suggest that the adsorption mechanism of the dextran is not changing between the asdeposited, amorphous surface and the annealed surface, but rather the annealing of the MoS₂ results in a decrease in the total number of favorable (hydrophobic) adsorption sites in which the dextran can adsorb onto the surface. This decrease in adsorption sites results in a slower adsorption rate of the polymer onto the surface and a decrease in the magnitude of the frequency and dissipation shifts. Further investigations are required to fully understand the mechanisms driving the dextran adsorption onto the surface and differences in adsorption behavior between the as-deposited and annealed surfaces. However, the deposition procedures described here allow the opportunity to further study these adsorption mechanisms on MoS₂ using both QCM-D analysis, as well as other planar surface characterization methods such as ellipsometry.

4. Conclusion

Here, we have developed a method for preparing molybdenum disulfide films onto commercially available Au QCM-D sensors and demonstrated their application for studying the adsorption behavior and conformation of polymers at the solid/liquid interface. Uniform MoS₂ films are deposited with well-controlled thicknesses from a single precursor through a novel pulse-deposition electrochemical reaction. The QCM-D sensors can be subsequently annealed to drive a phase transition of the as-deposited MoS₂ film from the amorphous phase to the 2H semiconducting phase without damaging the quartz crystal.

The exploration of new polymer or small molecule additives for froth flotation has largely relied on small-batch flotation methods and *ex situ* measurements of polymer conformation and coverage to determine their efficacy. While these methods are effective for probing the efficacy of an additive in producing the desired flota-

tion/suppression result, they often lack the ability to explore adsorption with a small affinity. Our exploration into the adsorption of dextran onto amorphous and crystalline MoS₂ surface demonstrate the ability to apply QCM-D to gain insight into the short-term kinetics of interaction between molecules and mineral surface, behavior that is key to designing additives with superior separation efficiency. The high sensitivity of QCM-D to small changes in polymer affinity will enable further explorations into the relationship between polymer structure and composition, and the adsorption of polymers onto molybdenum disulfide surfaces.

While the focus of this investigation has been on developing of molybdenum disulfide surfaces, expanding the library of mineral surfaces available on QCM-D sensors would greatly improve the ability to studying small molecule and polymeric adsorption at representative solid/liquid interfaces. Here, we have demonstrated the formation of MoS₂ films through an electrochemical deposition from a single precursor using a 2e⁻ decomposition reaction. Similar 2e⁻ decomposition reactions have been reported in the literature for forming alternative sulfide films and surfaces, including the deposition of copper sulfide thin films [34–36]. Applying the pulse deposition protocols developed here to these alternative mineral systems could expand the application of QCM-D measurements to study the adsorption of polymer and small molecule additives onto a variety of mineral surfaces with well-defined structures, compositions, and roughnesses. Furthermore, the protocols developed here for forming MoS2 films on QCM-D sensors could be applied to a variety of applications beyond froth flotation. For example, molybdenum disulfide is a promising material for electrochemical hydrogen production due to its high activity and stability [37]. Molybdenum disulfide coated QCM-D sensors could provide the opportunity to explore the chemical reaction rates of the molybdenum disulfide surface during this hydrogen evolution reaction.

CRediT authorship contribution statement

Christopher S. O'Bryan: Conceptualization, Methodology, Investigation, Visualization, Data curation, Formal analysis, Writing – original draft. Joseph Rosenfeld: Software, Visualization, Writing – original draft. Aria Zhang: Investigation, Visualization, Writing – original draft. Austin W. Keller: Investigation, Visualization, Writing – original draft. Denis Bendejacq: Conceptualization, Resources, Writing – review & editing. Cherie R. Kagan: Supervision. Christopher B. Murray: Supervision. Daeyeon Lee: Supervision, Project administration, Funding acquisition, Writing – review & editing, Conceptualization. Russell J. Composto: Supervision, Project administration, Funding acquisition, Writing – review & editing, Conceptualization.

Declaration of Competing Interest

The authors declare that they have no known competing financial interests or personal relationships that could have appeared to influence the work reported in this paper.

Acknowledgments

Funding for this study was provided by Solvay USA Inc., through Complex Assemblies of Soft Matter (COMPASS) international research laboratory IRL 3254. The authors would like to acknowledge primary support from MRSEC-DMR-1720530 as well as the associated shared experimental facilities. Support was also provided by the National Science Foundation Partnerships for International Research and Education Program (NSF-PIRE), Grant #1545884. Additional support of this work was provided by the

polymers-DMR1905912 (R.J.C) and the Semiconductor Research Corporation (SRC), Task 2797.001 (A.W.K.). In addition, we would like to acknowledge the Nanoscale Characterization Facility and the Scanning and Local Probe Facility at the Singh Center for Nanotechnology. Finally, the authors would like to thank Chengyu Wen for his assistance in annealing the samples.

Appendix A. Supplementary material

Supplementary data to this article can be found online at https://doi.org/10.1016/j.jcis.2022.01.098.

References

- M.C. Fuerstenau, G.J. Jameson, R.-H. Yoon, Froth flotation: a century of innovation, SME (2007).
- [2] R.J. Pugh, Macromolecular organic depressants in sulphide flotation—a review, 1, Principles, types and applications, International Journal of Mineral Processing 25 (1-2) (1989) 101–130.
- [3] C. Abarca, M.M. Ali, R.H. Pelton, Choosing mineral flotation collectors from large nanoparticle libraries, J. Colloid Interface Sci. 516 (2018) 423–430.
- [4] N.O. Lotter, D.J. Bradshaw, The formulation and use of mixed collectors in sulphide flotation, Miner. Eng. 23 (11-13) (2010) 945-951.
- [5] B. McFadzean, P. Dicks, G. Groenmeyer, P. Harris, C. O'Connor, The effect of molecular weight on the adsorption and efficacy of polysaccharide depressants, Miner. Eng. 24 (5) (2011) 463–469.
- [6] B. Triffett, C. Veloo, B.J.I. Adair, D. Bradshaw, An investigation of the factors affecting the recovery of molybdenite in the Kennecott Utah Copper bulk flotation circuit, Miner. Eng. 21 (12-14) (2008) 832–840.
- [7] G.-y. Liu, Y.-P. Lu, H. Zhong, Z.-F. Cao, Z.-h. Xu, A novel approach for preferential flotation recovery of molybdenite from a porphyry copper–molybdenum ore, Miner. Eng. 36-38 (2012) 37–44.
- [8] L. Guang-yi, Z. Hong, X. Liu-yin, W. Shuai, X.u. Zheng-he, Improving copper flotation recovery from a refractory copper porphyry ore by using ethoxycarbonyl thiourea as a collector. Miner. Eng. 24 (8) (2011) 817–824.
- ethoxycarbonyl thiourea as a collector, Miner. Eng. 24 (8) (2011) 817–824.

 [9] M. Kor, P.M. Korczyk, J. Addai-Mensah, M. Krasowska, D.A. Beattie, Carboxymethylcellulose adsorption on molybdenite: the effect of electrolyte composition on adsorption, bubble–surface collisions, and flotation, Langmuir 30 (40) (2014) 11975–11984.
- [10] A. Beaussart, L. Parkinson, A. Mierczynska-Vasilev, D.A. Beattie, Adsorption of modified dextrins on molybdenite: AFM imaging, contact angle, and flotation studies, J. Colloid Interface Sci. 368 (1) (2012) 608–615.
- [11] R.S.C. Smart, Innovations in measurement of mineral structure and surface chemistry in flotation: Past, present, and future, Society for Mining, Metallurgy and Exploration, 2014.
- [12] A. Ansari, M. Pawlik, Floatability of chalcopyrite and molybdenite in the presence of lignosulfonates, Part I. Adsorption studies, Minerals engineering 20 (6) (2007) 600–608.
- [13] A. Ansari, M. Pawlik, Floatability of chalcopyrite and molybdenite in the presence of lignosulfonates. Part II. Hallimond tube flotation, Miner. Eng. 20 (6) (2007) 609–616.
- [14] Q. Chen, S. Xu, Q. Liu, J. Masliyah, Z. Xu, QCM-D study of nanoparticle interactions, Adv. Colloid Interface Sci. 233 (2016) 94–114.
 [15] I.G. Sedeva, R. Fetzer, D. Fornasiero, J. Ralston, D.A. Beattie, Adsorption of
- [15] I.G. Sedeva, R. Fetzer, D. Fornasiero, J. Ralston, D.A. Beattie, Adsorption of modified dextrins to a hydrophobic surface: QCM-D studies, AFM imaging, and dynamic contact angle measurements, J. Colloid Interface Sci. 345 (2) (2010) 417–426.

- [16] Y. Hou, A. Sobhy, Y. Wang, Significance of reagents addition sequence on iron anionic reverse flotation and their adsorption characteristics using QCM-D, Physicochemical Problems of Mineral Processing 57 (1) (2021) 284–293.
- [17] J. Kou, S. Xu, In situ kinetics and conformation studies of dodecylamine adsorption onto zinc sulfide using a quartz crystal microbalance with dissipation (QCM-D), Colloids Surf., A 490 (2016) 110–120.
- [18] K. Shrimali, X. Yin, X. Wang, J.D. Miller, Fundamental issues on the influence of starch in amine adsorption by quartz, Colloids Surf., A 522 (2017) 642–651.
- [19] F. Teng, Q. Liu, H. Zeng, In situ kinetic study of zinc sulfide activation using a quartz crystal microbalance with dissipation (QCM-D), J. Colloid Interface Sci. 368 (1) (2012) 512–520.
- [20] N. Li, Q. Huang, J. Nie, X. Meng, Z. Wang, Y. Wu, M. Qi, Z. Liu, B. Mi, L. Lin, Dew point measurements using montmorillonite (MTT) and molybdenum disulfide (MoS2) coated QCM sensors, Sensors and Actuators B: Chemical 279 (2019) 122–129.
- [21] T. Jurca, M.J. Moody, A. Henning, J.D. Emery, B. Wang, J.M. Tan, T.L. Lohr, L.J. Lauhon, T.J. Marks, Low-temperature atomic layer deposition of MoS2 films, Angewandte Chemie International Edition 56 (18) (2017) 4991–4995.
- [22] S. Thomas, D.E. Smith, V.K. Greenacre, Y.J. Noori, A.L. Hector, C.H.(.d. Groot, G. Reid, P.N. Bartlett, Electrodeposition of MoS2 from Dichloromethane, J. Electrochem. Soc. 167 (10) (2020) 106511, https://doi.org/10.1149/1945-7111/ab9c88.
- [23] D. Johannsmann, The quartz crystal microbalance in soft matter research, Soft and Biological Matter (2015) 191–204.
- [24] M.C. Dixon, Quartz crystal microbalance with dissipation monitoring: enabling real-time characterization of biological materials and their interactions, Journal of biomolecular techniques: JBT 19 (3) (2008) 151.
- [25] E.A. Ponomarev, M. Neumann-Spallart, G. Hodes, C. Lévy-Clément, Electrochemical deposition of MoS2 thin films by reduction of tetrathiomolybdate, Thin Solid Films 280 (1-2) (1996) 86–89.
- [26] A.S. Aliyev, M. Elrouby, S.F. Cafarova, Electrochemical synthesis of molybdenum sulfide semiconductor, Mater. Sci. Semicond. Process. 32 (2015) 31–39.
- [27] M. Rodahl, B. Kasemo, On the measurement of thin liquid overlayers with the quartz-crystal microbalance, Sens. Actuators, A 54 (1–3) (1996) 448–456.
- [28] H. Li, Q. Zhang, C.C.R. Yap, B.K. Tay, T.H.T. Edwin, A. Olivier, D. Baillargeat, From bulk to monolayer MoS2: evolution of Raman scattering, Adv. Funct. Mater. 22 (7) (2012) 1385–1390.
- [29] S.M. Shapiro, D.C. O'Shea, H.Z. Cummins, Raman scattering study of the alphabeta phase transition in quartz, Phys. Rev. Lett. 19 (7) (1967) 361–364.
- [30] B. Schönfeld, J. Huang, S. Moss, Anisotropic mean-square displacements (MSD) in single-crystals of 2H-and 3R-MoS2, Acta Crystallographica Section B: Structural Science 39 (4) (1983) 404–407.
- [31] L. Xie, J. Wang, J. Huang, X. Cui, X. Wang, Q. Liu, H. Zhang, Q. Liu, H. Zeng, Anisotropic polymer adsorption on molybdenite basal and edge surfaces and interaction mechanism with air bubbles, Front. Chem. 6 (2018) 361.
- [32] A. Beaussart, A. Mierczynska-Vasilev, D.A. Beattie, Adsorption of dextrin on hydrophobic minerals, Langmuir 25 (17) (2009) 9913–9921.
- [33] Y. Hussain, J. Krim, C. Grant, OTS adsorption: A dynamic QCM study, Colloids Surf., A 262 (1-3) (2005) 81–86.
- [34] T. Martino, J. Smith, J. Chen, Z. Qin, J.J. Noël, D.W. Shoesmith, The properties of electrochemically-grown copper sulfide films, J. Electrochem. Soc. 166 (2) (2019) C9–C18.
- [35] A. Ghahremaninezhad, E. Asselin, D.G. Dixon, Electrodeposition and growth mechanism of copper sulfide nanowires, The Journal of Physical Chemistry C 115 (19) (2011) 9320–9334.
- [36] M. Lancaster, R. Mow, J. Liu, Q. Cheek, M.M. MacInnes, M.M. Al-Jassim, T.G. Deutsch, J.L. Young, S. Maldonado, Protection of GaInP2 Photocathodes by Direct Photoelectrodeposition of MoS x Thin Films, ACS Appl. Mater. Interfaces 11 (28) (2019) 25115–25122.
- [37] D. Voiry, M. Salehi, R. Silva, T. Fujita, M. Chen, T. Asefa, V.B. Shenoy, G. Eda, M. Chhowalla, Conducting MoS2 nanosheets as catalysts for hydrogen evolution reaction, NANO letters 13 (12) (2013) 6222–6227.